AIMS Materials Science, 3(3): 796-807.
DOI:10.3934/matersci.2016.3.796
Received: 04 June 2016
Accepted: 30 June 2016
Published: 04 July 2016

http://www.aimspress.com/journal/Materials

Research article

Spectroscopic and luminescent properties of Co^{2+}doped tin oxide thin films by spray pyrolysis

K. Ravindranadh [1], K. Durga Venkata Prasad [1], and M.C. Rao [2,*]

[1] Physics Division, Department of Basic Sciences & Humanities, Chirala Engineering College, Chirala-523 157, India
[2] Department of Physics, Andhra Loyola College, Vijayawada - 520 008, India

* **Correspondence:** Email: raomc72@gmail.com; Tel: 0866-2453485.

Abstract: The wide variety of electronic and chemical properties of metal oxides makes them exciting materials for basic research and for technological applications alike. Oxides span a wide range of electrical properties from wide band-gap insulators to metallic and superconducting. Tin oxide belongs to a class of materials called Transparent Conducting Oxides (TCO) which constitutes an important component for optoelectronic applications. Co^{2+}doped tin oxide thin films were prepared by chemical spray pyrolysis synthesis and characterized by powder X-ray diffraction, SEM, TEM, FT-IR, optical, EPR and PL techniques to collect the information about the crystal structure, coordination/local site symmetry of doped Co^{2+} ions in the host lattice and the luminescent properties of the prepared sample. Powder XRD data revealed that the crystal structure belongs to tetragonal rutile phase and its lattice cell parameters are evaluated. The average crystallite size was estimated to be 26 nm. The morphology of prepared sample was analyzed by using SEM and TEM studies. Functional groups of the prepared sample were observed in the FT-IR spectrum. Optical absorption and EPR studies have shown that on doping, Co^{2+} ions enter in the host lattice as octahedral site symmetry. PL studies of Co^{2+} doped SnO_2 thin films exhibit blue and yellow emission bands. CIE chromaticity coordinates were also calculated from emission spectrum of Co^{2+} doped SnO_2 thin films.

Keywords: SnO_2; spray pyrolysis; copper ions; TEM; optical absorption; EPR; photoluminescence

1. Introduction

In recent years, nanotechnology endorsed high desire to old areas of knowledge due to simple reduction of crystallite size. New morphologies have been created, prominent to an increase in performance or changes in mechanical, chemical and electrical properties of materials. With reduction in the size of material its properties are dynamically changed [1]. Semiconductor materials are widely used in electronic devices but in the field of optoelectronics these materials have some limitations. To overcome these limitations metal oxides are used. Transition metal oxides with assorted structures, properties and phenomena have been the focus of much attention in recent years in view of their scientific and technological applications [2].

Semiconductor oxide thin films are materials with abundant solicitations in electronic and optoelectronic devices as well as some other applications such as protective coatings, heat mirrors and catalysis [3–5]. In the context of world energy demand, particularly energy conversion, transparent conductive oxides (TCOs) based on semiconductor oxides, play a crucial role in the development of new fashioned luminescent materials and thin film solar cells [6].Tin oxide (SnO_2) is a special oxide material because it has a low electrical resistance with high optical transparency in the visible range. Due to these properties, apart from gas sensors, SnO_2 is being used in many other applications, such as electrode materials in solar cells, light-emitting diodes, flat-panel displays and other optoelectronic devices where an electric contact needs to be made without obstructing photons from either entering or escaping the optical active area and in transparent electronics, such as transparent field effect transistors [7–25].

Usually semiconductor oxide hosts are incorporated with small concentrations of activator ions, transition (3d) or rare-earth (4f) metals. The absorption and emission bands of activators are controlled by changing the crystal field or covalence depending on sitesymmetry and coordination number of activator ions [26]. Among the 3d transition metal ions, cobalt ions can show an efficient luminescence property [27].SnO_2 thin films have been deposited using different techniques, such as spray pyrolysis [28], sol-gel process [29], chemical vapour deposition [30], sputtering [31] and pulsed laser deposition [32].Among these, spray pyrolysis is the most convenient method because of its simplicity, low cost, easy to add doping materials and the possibility of varying the film properties by changing composition of starting solution. In the present work, Co^{2+} doped (0.01 mol%) SnO_2 thin films were prepared by using chemical spray pyrolysis method. The prepared thin films were characterized by powder X-ray diffraction, SEM, TEM, FT-IR, optical, EPR and PL studies to collect the information about the structural and luminescent properties of the prepared sample.

2. Materials and Method

2.1. Materials and Synthesis

SnO_2 and Cobalt oxide (CoO) were purchased from Merck Chemicals. All the chemical reagents used in this experiment were analytical grade and used without further purification.Co^{2+} doped SnO_2 thin films were prepared by chemical spray pyrolysis. Spray solution was prepared by mixing 0.1 M aqueous solution of SnO_2 and CoO (0.01 mol%) using magnetic stirrer.

$$3x\ SnO_2 + CoO \xrightarrow{673\ K} Sn_{3x}CoO_x + 2x\ O_2 \uparrow \text{ (Where x = 68.9)}$$

The automated spray solution was then transferred to the hot substrate kept at the normalized deposition temperature of 673 K using filtered air as carrier gas at a flow rate normalized to approximately 1.8 ml/min. To prevent the substrate from excessively cooling, the prepared solution was sprayed on the substrate for 10 s with 15 s intervals. The films deposited onto micro-glass slides were first cleaned with detergent water and then dipped in acetone.

2.2. Characterization

Powder X-ray diffraction pattern of the prepared samples are recorded on PANalytical Xpert Pro diffractometer with CuKα radiation. Scanning electron microscope (SEM) and energy dispersive spectrum (EDS) images are taken on ZEISS EVO 18. Transmission electron microscope (TEM) images are recorded on HITACHI H-7600 and CCD CAMERA system AMTV-600 by dispersing samples in ethanol. Bruker FT-IR spectrophotometer is used for recording FT-IR spectrum of the prepared samples in the region 400–4000 cm^{-1}. Optical absorption spectrum was obtained at room temperature using JASCO V-670 Spectrophotometer in the wavelength region of 200–1400 nm. Electron paramagnetic resonance (EPR) spectrum is obtained at room temperature on JEOL JES-FA series X-band EPR spectrometer having 100 kHz field modulation. Photoluminescence (PL) spectrum is taken at room temperature on Horiba Jobin-Yvon Fluorolog-3 spectrofluorimeter with Xe continuous (450 W) and pulsed (35 W) lamps as excitation sources.

3. Results and Discussion

Co^{2+} doped (0.01 mol%) SnO_2 thin films were prepared by using chemical spray pyrolysis method. The prepared thin films were characterized by powder X-ray diffraction, SEM with EDS, TEM, FT-IR, optical, EP Rand PL studies to collect the information about the spectroscopic and luminescent properties of prepared sample. The analysis of X-ray diffraction pattern revealed that the prepared tin oxides films are pure crystalline in nature.

3.1. Structural Properties

3.1.1. Powder X-ray diffraction Studies

Figure 1 shows the X-ray diffraction pattern of Co^{2+} doped SnO_2thin films. The XRD pattern of these optimized samples is in good agreement with the reference pattern of tin oxide with standard diffraction data of JCPDS file No.41-1445.The diffraction data is indexed to tetragonal rutile phase of tin oxide which belongs to the space group $P4_2/mnm$and the corresponding lattice cell parameters are evaluated as a = b = 0.471 nm and c = 0.317 nm. The analysis of X-ray diffraction pattern revealed that the prepared tin oxides films are pure crystalline in nature. It is perceptible from the XRD pattern of Co^{2+}doped tin oxide films grow along the preferred orientation of (110).The average crystallite size of the prepared sample is calculated by using Debye-Scherrer's formula,

$$\mathbf{D = (k\lambda/\beta\cos\theta)}$$

where k is a constant (about 0.9), λ is wavelength of X-ray radiation (1.5405Å), β is full width at half maximum (FWHM) intensity of the diffraction line and θ is diffraction angle. Based on the value of FWHM, the average crystallite size is estimated to be 26 nm, which is in the order of nanosize.

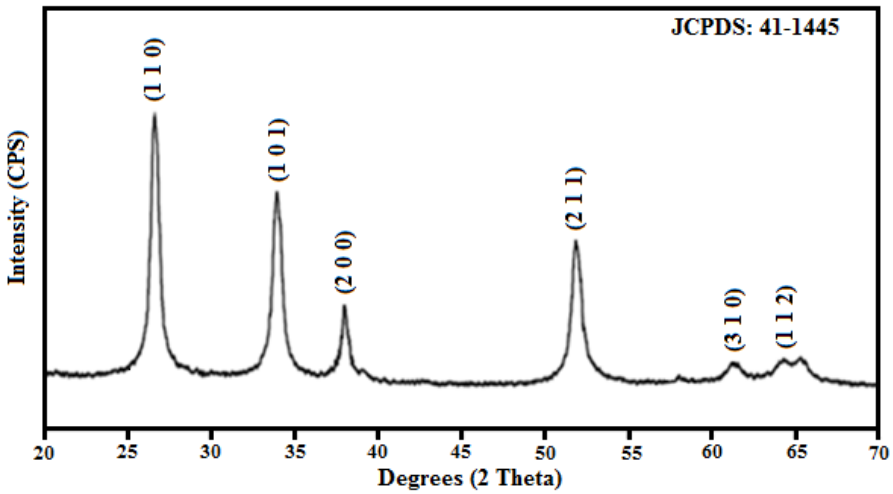

Figure 1. Powder X-ray diffraction pattern of Co^{2+} doped SnO_2 thin films.

3.1.2. Morphological Studies

The morphology and chemical composition of as synthesized thin film was investigated by SEM and EDS analysis. Figure 2 shows the SEM micrographs of Co^{2+} doped SnO_2 thin films taken with different magnifications. It can be clearly observed from low resolution SEM images that, the prepared sample shows agglomeration with an irregular morphology. The agglomeration could be induced by densification resulting from the narrow space between particles. SEM images reveal that the sample consists of irregular shaped sphere like structures. The assimilation of copper into the host material was confirmed by EDS measurements. The observed EDS pattern was shown in Figure 3. The pattern showed the elemental compositions of Sn, O and cobalt. From this it was confirmed that the prepared samples contains doped cobalt species. TEM measurements were performed to confirm the nanocrystalline nature of the samples and to study the morphology of the particles. The TEM images of Co^{2+} doped SnO_2 thin films are depicted in Figure 4. The particles are more or less uniformed in size and of irregular shape.

3.1.3. FT-IR Studies

FT-IR spectrometry was used for the determination of existing surface species. The FT-IR spectrum of Co^{2+} doped SnO_2 thin films was illustrated in Figure 5. The bands at the low wavenumbers (500–1000 cm^{-1}) could be attributed to SnO_2. The peaks at 675, 787 and 963 cm^{-1} were assigned to O–Sn–O, Sn–O–Sn stretching vibrations and lattice vibrations, while the peaks at 568 and 865 cm^{-1} were due to Sn–OH bonds of the SnO_2 crystalline phase [33]. The bands observed in the region 2500–1640 cm^{-1} are due to symmetric and asymmetric vibrations of hydroxyl ions situated at different sites in the lattice.

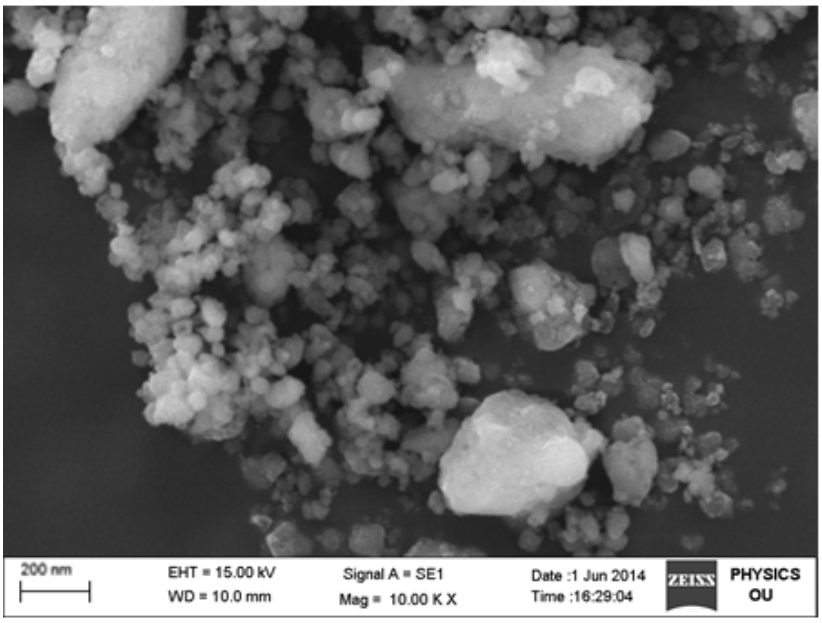

Figure 2. SEM image of Co^{2+} doped SnO_2 thin films.

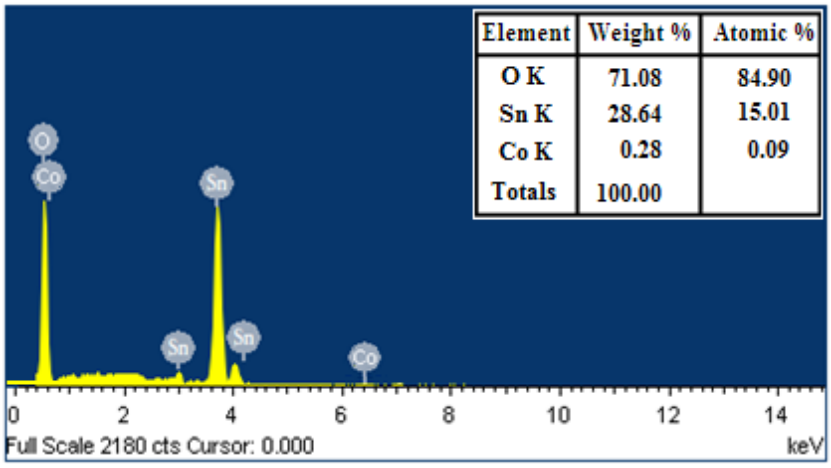

Figure 3. EDS spectrum of Co^{2+} doped SnO_2 thin films.

3.2. Optical Properties

3.2.1. Optical Absorption Studies

Optical absorption spectra of Co^{2+} doped SnO_2 a thin film at room temperature is shown in Figure 6. The spectra exhibit six absorption bands at around 1195, 631, 558, 494, 442 and 385 nm. These bands are assigned to various transitions of Co^{2+} in octahedral site symmetry. For Co^{2+} (d^7) in octahedral field without spin-orbit interaction, three spin allowed transitions are to be expected and they are $^4T_{1g}(F) \rightarrow {}^4T_{2g}(F)$, $^4T_{1g}(F) \rightarrow {}^4A_{2g}(F)$ and $^4T_{1g}(F) \rightarrow {}^4T_{1g}(P)$. Of these transitions $^4T_{1g}(F) \rightarrow {}^4A_{2g}(F)$ involves the promotion of two electrons and is expected to be weak [34]. Accordingly, other three bands are attributed to transitions $^4T_{1g}(F) \rightarrow {}^2A_{1g}(G)$, $^2T_{1g}(G)$ and $^2A_{1g}(F)$ respectively. In O_h symmetry theoretically the ratios of energies of transitions $^4T_{1g}(F) \rightarrow {}^4A_{2g}(F)$: ν_2 and $^4T_{1g}(F) \rightarrow$

$^4T_{2g}(F)$: ν_1 are almost invariable from 1.9 to 2.2 [35,36]. In the present study, ratio of ν_2 to ν_1 is around 2.14. The energy matrix for d^7 configuration is solved for different sets of crystal field (Dq) and inter-electronic repulsion (B and C) parameters. These parameters give good fit with the observed band positions at Dq = 945 and B = 850, C = 3750 cm^{-1}.

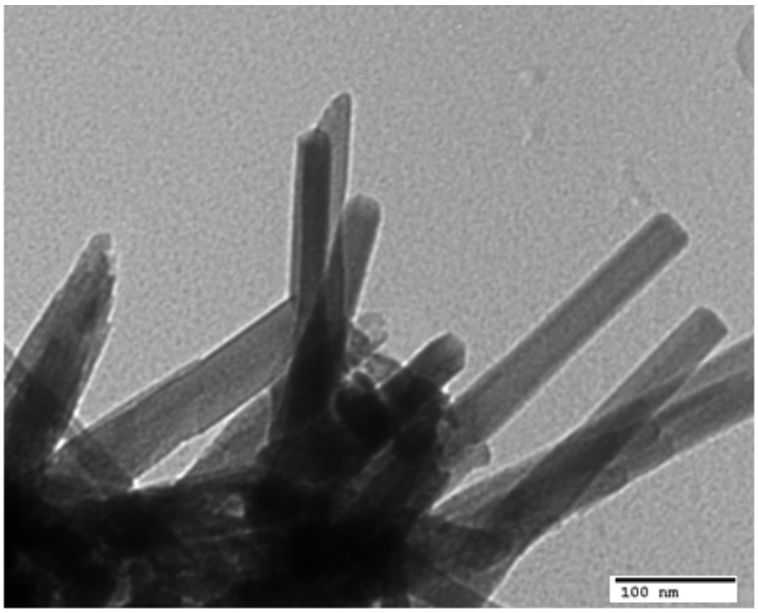

Figure 4. TEM image of Co^{2+} doped SnO_2 thin films.

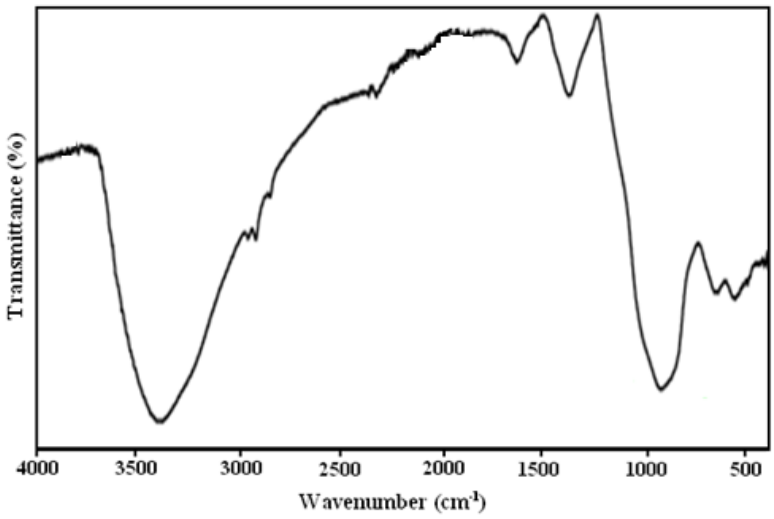

Figure 5. FT-IR spectrum of Co^{2+} doped SnO_2 thin films.

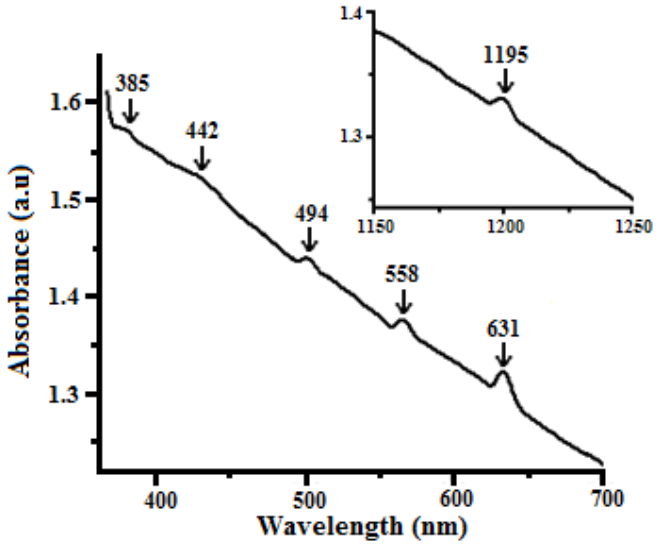

Figure 6. Optical absorption spectrum of Co^{2+} doped SnO_2 thin films.

3.2.2. EPR Studies

Electron paramagnetic resonance (EPR) spectroscopy is a method for characterizing structure, dynamics and spatial distribution of paramagnetic ions. Diamagnetic materials can be studied by using spin probes which are stable paramagnetic species such as nitroxide radicals and transition metal ions. Due to the presence of at least one unpaired electron many paramagnetic species are chemically active. Therefore EPR spectroscopy is a valuable technique for obtaining detailed information on the geometric and electronic structure of various materials. Generally EPR spectrum of Co^{2+} is observed only at low temperatures because the spin lattice relaxation time is extremely short for octahedral coordination of Co^{2+} ions. At higher temperature, the spectra become broader probably due to short relaxation time characteristic of the high spin state of Co^{2+} ions [37].In exact octahedral symmetry, the d^7 configuration has an orbital triplet state the lowest of which is split by spin-orbit coupling to give a ground state Kramers' doublet with g = 4.33 [38]. In the present investigations of Co^{2+} doped SnO_2 thin films, the room temperature characteristic EPR spectrum was shown in Figure 7. The spectrum exhibited unresolved single resonance signal at g = 2.7 which is an indication of Co^{2+} ions in distorted octahedral symmetry and this resonance is due to a random distribution of distortions in the sample [39–42].

By correlating EPR and optical absorption spectral data, the covalency parameter (k_0) is evaluated by following relation [43],

$$\mathbf{g = 3.33 + k_0 - 7.5\ (\lambda/\Delta)}$$

where g is observed g-factor, λ is spin-orbit coupling constant (−178 cm^{-1} for Co^{2+}) and Δ is energy difference between $^4T_{1g}(F) \rightarrow {}^4T_{2g}(F)$. Generally, k_0 value lies between 0.5 and 1.0, the limits of pure covalent and pure ionic bonding respectively. The calculated k_0 value is 0.78 which indicates that the bonding between the Co^{2+} ions and the ligands is moderately covalent nature.

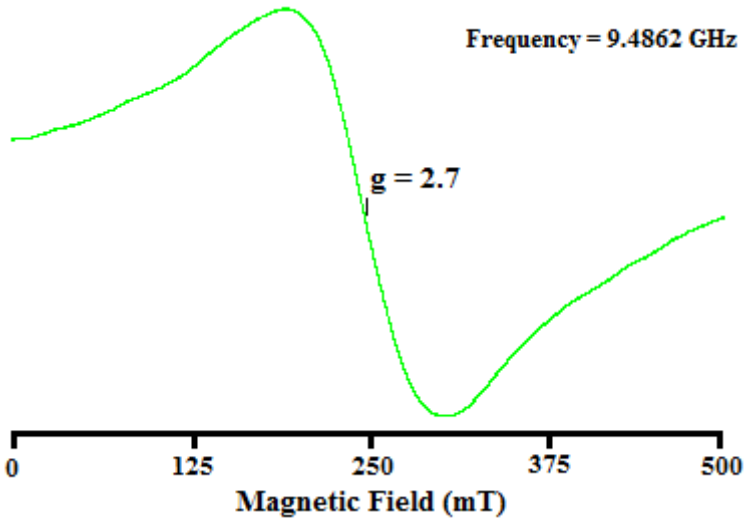

Figure 7.EPR spectrum of Co^{2+} doped SnO_2 thin films.

3.2.3. Photoluminescence Studies

Figure 8 shows the room temperature PL spectrum of Co^{2+} doped SnO_2 thin films under excitation wavelength of 325 nm.PL spectrum of Co^{2+}doped SnO_2 thin films exhibit broad band extending from 365 to 567 nm and peaking at 567 nm, which is due to electric-dipole allowed $^4A_{2g}(F) \rightarrow {}^4T_{1g}(F)$ transition of Co^{2+} ions. In this study, a sharp and dominated yellow emission at around 567 nm, a suppressed blue emission at around 425, 467 nm and a weak UV-visible emission at around 365 nm in Co^{2+}doped SnO_2 thin films indicate that the prepared samples have better crystal quality and good optical properties with less defect states. These characteristic features may represent possible applications in the fields of white-LEDs and display devices [41].

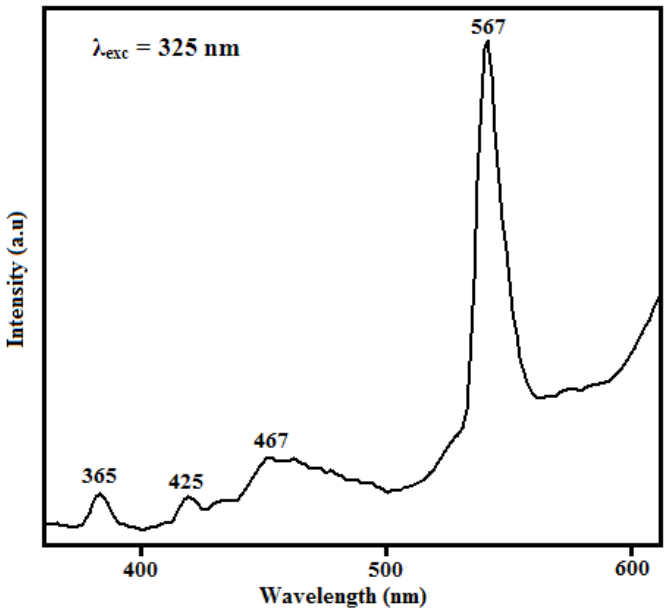

Figure 8. PL spectrum of Co^{2+} doped SnO_2 thin films.

3.2.4. Chromaticity Properties

Most lighting specifications refer to colour in terms of the 1931 Commission Internationale deI'Eclairage (CIE) chromatic colour coordinates which recognize that the human visual system uses three primary colours: red, green and blue [44].The colour purity of prepared sample depends on spectral energy distribution of emission. Generally, colour purity can be determined by measuring its (x,y) coordinates on a standard CIE colour chart. The colour gamut of a sample is represented as an area inthe CIE 1931 chromaticity diagram with curved edgerepresenting monochromatic colours [45].

The CIE 1931 chromaticitycoordinates of Co^{2+}doped SnO_2 thin films were calculated from emission spectrum. The location of colour coordinates for Co^{2+} dopedSnO_2 thin films in CIE chromaticity diagram is shown in Figure 9 by a solid circle sign (•). From this figure, one can see that the colour of Co^{2+} dopedSnO_2 thin films located in white region and the CIE coordinates are(x = 0.335, y = 0.363) respectively.

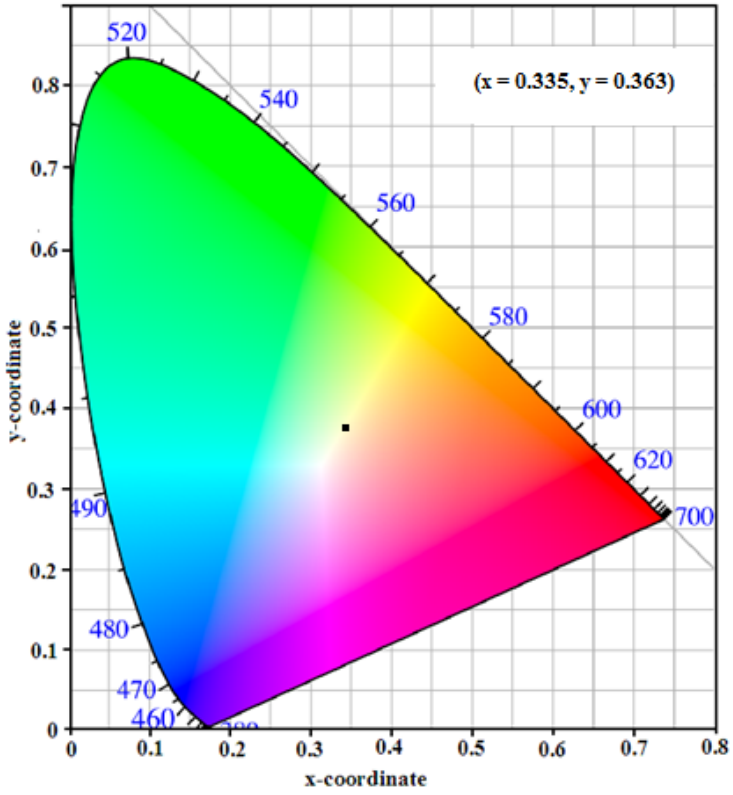

Figure 9. CIE diagram of Co^{2+} doped SnO_2 thin films.

In order to inspect the quality of light, colour correlated temperature (CCT) values have been calculated is given by the McCamy empirical formula [46];

$$\mathbf{CCT = - 437n^3 + 3601n^2 – 6861n + 5514.31}$$

where $n = (x-x_e)/(y-y_e)$ and the chromaticity epicenter is at $x_e = 0.3320$ and $y_e = 0.1858$.The CCT is an indication of colour appearance of light emitted by light source. Under long-wavelength UV

excitation, a set of fluorescence with colour temperatures varying from 5000 to 20000K can be applied to circadian lights. Generally, CCT value greater than 5000 K indicates the cold white light used for commercial lighting purpose and less than 5000 K indicates warm white light used for home applications [47]. In the present study, CCT value is 4267 K, which represents warm white light emission.

4. Conclusion

Co^{2+} doped SnO_2 thin films were prepared successfully by chemical spray pyrolysis method. From the powder X-ray diffraction study, the crystal system is indexed to tetragonal rutile phase and the lattice cell parameters are evaluated. The evaluated average crystallite size of Co^{2+} doped SnO_2 thin films is 26 nm.SEM micrographs shows irregular shaped sphere like structures and EDS analysis confirms the presence of constituent elements of the prepared material. TEM images clearly show the formation of nano rods. FT-IR spectrum showed the characteristic vibrational modes of host lattice. Optical absorption spectrum shows six characteristic bands, which are the characteristic of Co^{2+} in distorted octahedral symmetry. This was also confirmed from EPR studies, which shows a strong resonance signal at around 2.7 which is another evidence of Co^{2+}in octahedral symmetry.PL spectrum of Co^{2+} doped SnO_2 thin films shows strong yellow emission with suppressed blue emission. From CIE diagram, Co^{2+} doped SnO_2 thin films emits white colour light and the corresponding coordinates are (x = 0.335, y = 0.363). These materials may be useful for display and LED devices.

Conflict of Interest

All authors declare no conflict of interest in this paper.

References

1. Rao MC, Ravindranadh K, Shekhawat MS (2016) Structural and Electrical Properties of TiO_2 Thin films. *AIP Conf Proc* 1728: 020077.
2. Rao MC, Ravindranadh K, Kasturi A, et al. (2013)Structural Stoichiometry and Phase Transitions of MoO_3 Thin Films for Solid State Microbatteries. *Res J Rec Sci* 2: 67–73.
3. Granqvist CG (2007) Transparent conductors as solar energy materials: A panoramic review. *Sol Ener MaterSol Cells* 91: 1529–1598.
4. Exarhos GJ, Zhou XD (2007) Discovery-based design of transparent conducting oxide films. *Thin Solid Films* 515: 7025–7052.
5. Malato S, Fernández-Ibanez P, Maldonado MI, et al. (2009) Decontamination and disinfection of water by solar photocatalysis: recent overview and trends. *Catal Today* 147: 1–59.
6. Li B, Wang LD, Kang BN, et al. (2006) Review of recent progress in solid-state dye-sensitized solar cells. *Sol Ener Mater Sol Cells* 90: 549–573.
7. Wager JF (2003) Transparent electronics. *Science* 300: 1245–1246.
8. Rao MC, Hussain OM (2010) Synthesis and electrochemical properties of Ti doped $LiCoO_2$ thin film cathodes. *J Alloys Comp* 491: 503–506.

9. Rao MC (2011) Fabrication of $LiCoO_2$, $LiTi_xCo_{1-x}O_2$ and $LiNi_xCo_{1-x}O_2$ thin film cells for rechargeable lithium microbatteries. *Optoelect Adv Mater (Rapid Commu)* 5: 85–88.
10. Rao MC (2010) Growth and microstructural features of laser ablated $LiCoO_2$ thin films. *J Crys Growth* 312: 2799–2803.
11. Rao MC, Hussain OM (2009) Optical and electrical properties of laser ablated amorphous $LiCoO_2$ thin film cathodes. *IOP Conf Series Mater Sci Eng* 2: 012037.
12. Rao MC, Hussain OM (2009) Spectroscopic investigations on tetravalent doped $LiCoO_2$ thin film cathodes. *Eur Phys J Appl Phys* 48: 20503.
13. Rao MC, Hussain OM (2011) Optical and electrical properties of $LiNi_xCo_{1-x}O_2$ thin films. *Optoelect Adv Mater* 13: 1109–1113.
14. Rao MC (2012) Microfabrication of $LiCoO_2$ thin film cell. *Int J Chem Sci* 10: 1111–1116.
15. Rao MC (2012) Effect of target composition on the growth of stiochiometric $LiCoO_2$, $LiTi_xCo_{1-x}O_2$ and $LiNi_xCo_{1-x}O_2$ thin films. *Optoelect Adv Mater (Rapid Commu)* 5: 651–654.
16. Rao MC (2011) Grain size effect on the growth of $LiCoO_2$ thin film cathodes. *J Optoelect Adv Mater* 13: 428–431.
17. Rao MC (2012) Synthesis and characterization of $LiCoO_2$ thin film cathodes grown by pulsed laser deposition. *Optoelect Adv Mater (Rapid Commu)* 6: 511–515.
18. Rao MC (2011) Spectroscopic investigations on laser ablated $LiNi_xCo_{1-x}O_2$ thin films. *J Optoelect Adv Mater* 13: 78–81.
19. Muntaz Begum Sk, Rao MC, Ravikumar RVSSN (2013) Cu^{2+} doped PVA passivated ZnSe nanoparticles - preparation, characterization and properties. *J Inorg Organometa Poly Mater* 23: 350–356.
20. Muntaz Begum Sk, Rao MC, Ravikumar RVSSN (2011) Physical and spectral investigations of Mn^{2+} ions doped poly vinyl alcohol capped ZnSe nanoparticles. *J Mol Struct* 1006: 344–347.
21. Muntaz Begum Sk, Rao MC, Ravikumar RVSSN (2012) Spectroscopic investigations of Fe^{3+} doped poly vinyl alcohol (PVA) capped ZnSe nanoparticles. *Spectrochim Acta A* 98: 100–104.
22. Ravindranadh K, Rao MC, Ravikumar RVSSN (2015) EPR and optical studies of Fe^{3+} doped Ca-Li hydroxyapatite nanopowder- mechanochemical synthesis. *Appl Mag Reson* 46: 1–15.
23. Ravindranadh K, Rao MC, Ravikumar RVSSN (2015) Optical and structural properties of undoped and Mn^{2+} doped Ca-Li hydroxyapatite nanopowders using mechanochemical synthesis. *J Luminesce* 159: 119–127.
24. Hoffman RL, Norris BJ, Wager JF (2003) ZnO-based transparent thin-film transistors. *Appl Phys Lett* 82: 733–735.
25. Rao MC, Ravindranadh K, Satyanarayana T, et al. (2016) Luminescent and Gas Sensing Properties of SnO_2 Thin Films Grown by Pulsed Laser Deposition. *Der Phar Chem* 8: 243–250.
26. Henderson B, Imbush GG (1989) Optical Spectroscopy of Inorganic Solids, Clarendon Press, Oxford.
27. Ravindranadh K, Babu B, Jaesool Shim, et al. (2015) Structural and Photoluminescence Studies of Co^{2+} doped Ca-Li Hydroxyapatite Nanopowders. *J Mater Sci Mater Elec* 26: 6667–6675.
28. Shinde SD, Patil GE, Kajale DD, et al. (2012) synthesis of ZnO nano rods for spay pyrolysis for H_2S gas sensor.*J Alloys Compd* 528: 109–114.
29. Cobianu C, Savaniu C, Siciliano P, et al. (2001) SnO_2 sol-gel derived thin films for integrated gas sensors. *Sens Actuators B*77: 496–502.

30. Larciprete R,Borsella E, De Padova P, et al. (1998)Organotin films deposited by laser-induced CVD as active layers in chemical sensors. *Thin Solid Films* 323: 291–295.
31. Sberveglieri G, Faglia G, Groppelli S, et al. (1992) Methods for the preparation of NO, NO_2 and H_2 sensors based on tin oxide thin films, grown by means of the rf magnetron sputtering technique. *Sens Actuators B* 8: 79–88.
32. Dolbec R, El Khakani MA, Serventi AM, et al. (2003) Influence of the nanostructural characteristics on the gas sensing properties of pulsed laser deposited tin oxide thin films. *Sens Actuators B* 93: 566–571.
33. Khan AF, Mehmood M, AslamM, et al. (2010) Characteristics of electron beam evaporated nanocrystalline SnO_2 thin films annealed in air. *Appl Surf Sci* 256: 2252–2258.
34. Jones GD (1967) Jahn-Teller Splittings in the Optical Absorption Spectra of Divalent Iron Compounds. *Phys Rev* 155: 259–285.
35. Babu B, Aswani T, Thirumala Rao G, et al. (2014) Room temperature ferromagnetism and optical properties of Cu^{2+} doped ZnO nanopowder by ultrasound assisted solid state reaction technique. *J Magn Magn Mater* 355: 76–80.
36. Benhaliliba M, Benouis CE, Tiburcio-Silver A, et al. (2012) Luminescence and physical properties of copper doped CdO derived nanostructures. *J Lumin* 132: 2653–2658.
37. Sonawane YS, Kanade KG, Kale BB, et al. (2008) Electrical and gas sensing properties of self-aligned copper-doped zinc oxide nanoparticles. *Mater Res Bull* 43: 2719–2726.
38. Karamat S, Rawat RS, Tan TL, et al. (2013) Exciting Dilute Magnetic Semiconductor: Copper-Doped ZnO. *J Supercond Novel Magn* 26: 187–195.
39. Rapacz-Kmita A, Paluszkiewicz C, Slosarczyk A, et al. (2005) FTIR and XRD evaluation of carbonated hydroxyapatite powders synthesized by wet methods. *J Mol Struct* 744: 657–661.
40. Rama Krishna Ch, Ravikumar RVSSN (2014) Synthesis and characterization of vanadium ions containing chloro-cadmium phosphate $CdHPO_4Cl[H_3N(CH_2)_6NH_3]_{0.5}$ crystals. *Physica B* 433: 7–11.
41. Fathi MH, MohammadiZahrani E (2009) Mechanical alloying synthesis and bioactivity evaluation of nanocrystalline fluoridated hydroxyapatite. *J Cryst Growth* 311: 1392–1403.
42. Liu Y, Wang W, Zhan Y, et al. (2002) A simple route to hydroxyapatite nanofibers. *Mater Lett* 56: 496–501.
43. Smith DW (1970) Relationship between electron spin resonance *g*-values and covalent bonding in tetragonal copper(II) compounds. *J ChemSoc A* 3108–3120.
44. Rao MC, Ravindranadh K (2016) Optical and EPR Studies of Cu^{2+} Doped SnO_2 Thin Films by Spray Pyrolysis. *Mater Res Innov*.
45. Murugan R, Ramakrishna S (2005) Aqueous mediated synthesis of bioresorbable nanocrystalline hydroxyapatite. *J Cryst Growth* 274: 209–213.
46. Zhang H, Zhu Q, Xie Z (2005) Mechanochemical-hydrothermal synthesis and characterization of fluoridated hydroxyapatite. *Mater Res Bull* 40: 1326–1334.
47. Jaya RB, Rajesh YM, Pushpa MV, et al. (2015) Optical and Structural Investigations of Cu(II) ions doped $Li_2CaAl_4(PO_4)_4F_4$ Nanophosphors. *Appl Mag Res* 46: 953–964.